 doi:10.20944/preprints201809.0124.v1

Nanoplasmonic Sensing of $CH_3NH_3PbI_3$ Perovskite Formation in Mimic of Solar Cell Photoelectrodes

Fahd Rajab

Chemical Engineering Department, College of Engineering, Najran University, Saudi Arabia

Promising Centre for Sensors and Electronic Devices (PCSED), Advanced Materials and Nano-Research Centre, Najran University, P.O. Box: 1988, Najran 11001, Saudi Arabia.

Corresponding Author

* E. mail: fmrajab@nu.edu.sa; fahdrajab@gmail.com (Fahd Rajab)

Tel: +966-75428942; Fax: +966-75428887.

 doi:10.20944/preprints201809.0124.v1

Abstract

The formation of methylammonium lead iodide ($CH_3NH_3PbI_3$) perovskite into mesoporous titania (TiO_2) scaffold via a sequential deposition method is known to offer high quality films for good photovoltaic device performance. The growth reactions at the mesoporous TiO_2 film depend on reactants concentration in the host matrix and the reaction activation energy. Here, we have used a NanoPlasmonic Sensing (NPS) approach with gold (Au) nanosensors to monitor the formation of $CH_3NH_3PbI_3$ perovskite at the lower interface of 350 nm mesoporous TiO_2, typical thickness used in a photovoltaic device. This technique provides time-resolved spectral shifts of the localized surface plasmon resonance at different operating temperatures and methylammonium iodide ($CH_3NH_3I_3$) concentrations by recording changes in the local vicinity of the Au nanosensors at the mesoporous TiO_2 film interface. Analytical studies included Ellipsometry, Scanning Electron Microscopy, and X-ray diffraction. The results show that perovskite conversion can be obtained at lower $CH_3NH_3I_3$ concentrations if reaction activation energy is lowered. A significant finding is that the NPS response at 350 nm mesoporous TiO_2 can widely change from red shifts to blue shifts depending on extent of conversion and morphology of perovskite formed at given reaction conditions.

Keywords: Nanoplasmonic sensing spectroscopy; $CH_3NH_3PbI_3$ perovskite; Mesoporous TiO_2; Gold nanosensor

 doi:10.20944/preprints201809.0124.v1

1. Introduction

Perovskite solar cells based on alkylammonium metal trihalide light-absorption layer offer the promise for a breakthrough for next generation solar devices [1-7]. Methylammonium lead halides exhibit several advantages of unique optical characteristics with band gap tunability, high mobility and long carrier lifetime [8-13]. Mixed-halide perovskites have shown significant improvement in tuning the bandgap by adjusting the stoichiometry [14]. Formation dynamics of Methylammonium lead iodide has been found to be processing specific [10]. Perovskite films have been deposited either via thermal evaporation [15, 16], or solution processing [5, 11, 12]. The two common pathways often applied during film formation are one-step method in which the reactants are thoroughly mixed prior to deposition [17, 18] and two-step route where the precursors are sequentially deposited [1, 8, 13]. Control over perovskite morphology was observed using the two-deposition route to either thick or thin mesoscopic metal oxides [11, 12, 19]. The growth and fabrication conditions of these films significantly affect the performance of the fabricated photovoltaic devices especially for mixed-halide perovskites. While conversion of polycrystalline perovskite is preferred for solar cells, growth of single crystals into multi-dimensional shapes has gained much attention in recent years [18].

In prior work, Rajab et al [20] used nanoplasmonic sensing (NPS) to detect methylammonium lead iodide ($CH_3NH_3PbI_3$) perovskite at the interface of compact/650 nm mesoporous TiO_2 films with Au nanodisks, where complete conversion of perovskite formation was characterized by slow NPS red shifts compared with fast methylammonium iodide ($CH_3NH_3I_3$) crystallization in incomplete reactions. When complete reaction activation energies are reduced, perovskite formation was characterized by relatively fast

Preprints (www.preprints.org) | NOT PEER-REVIEWED | Posted: 7 September 2018 doi:10.20944/preprints201809.0124.v1

NPS red shifts. Overall NPS red shifts were primarily due to sufficient perovskite conversion required for dielectric constant change at the interface of the gold nanosensors.

In this paper, we demonstrate the use of NPS to detect the faster formation kinetics of $CH_3NH_3PbI_3$ perovskite at the interface of compact/350 nm mesoporous TiO_2 films with Au nanodisks. We monitor time-resolved spectral shifts of the Localized Surface Plasmon Resonance (LSPR) peak induced by the embedded plasmonic Au sensors. The rate constants of the compact/350 nm mesoporous TiO_2 films are orders of magnitude higher than in the previous studied compact/650 nm mesoporous TiO_2 films [20]. We assess the formed perovskite structures according to the analytical results obtained by the characterization techniques. Additionally, we characterize the growth of multi-dimensional objects by their NPS shifts and reaction rate constants.

2. Experimental

2.1.Materials

Insplorion sensors with a dense TiO_2 coating were purchased from Insplorion AB (Gothenburg, Sweden). TiO_2 paste (The average particle size 20 nm) was acquired from Dyesol. Lead iodide (PbI_2) and methyl ammonium iodide ($CH_3NH_3I_3$: MAI) were purchased from Solaronix. Dimethylformamide (DMF), propanol and ethanol were purchased from Sigma Aldrich.

2.2.Film formation

Standard films comprising of fused silica coated with Au nanodisks (100 nm diameter and 20 nm height) and 10 nm dense layer of compact TiO_2 as a dielectric spacer layer were used to analyze the nanoplasmonic sensing of Au nanosensors, similar to the early studied NPS experimental

Preprints (www.preprints.org) | NOT PEER-REVIEWED | Posted: 7 September 2018 doi:10.20944/preprints201809.0124.v1

system arrangements [21, 22, 23, 24]. These films were then spin-coated with mesoporous TiO_2 films prepared by mixing a commercial TiO_2 paste from dyesol and ethanol (2:7 wt %) at 5000 rpm for 30 s. The films are calcinated at 500 $^{\circ}$C for 30 min. The thickness of mesoporous TiO_2 films was confirmed using VASE Ellipsometer VB-400. Then, 1M (462 mg/mL) of lead iodide (PbI_2) in dimethylformamide (DMF) was prepared under stirring at 70 $^{\circ}$C. The mesoporous TiO_2 films were consequently infiltrated with PbI_2 by spin coating at 6000 rpm for 90 s and dried at 70 $^{\circ}$C for 30 min. Different concentrations of MAI in 2-propanol ranging from 5 to 15 mg/mL at various temperatures from 25 to 53°C were prepared for in situ monitoring of perovskite formation.

2.3 In situ nanoplasmonic sensing of $MAPbI_3$ perovskite formation

Insplorion Xnano was used to monitor nanoplasmonic peaks during $MAPbI_3$ perovskite formation as described elsewhere. [20] Initially, a blank measurement was taken for a fused silica substrate for subtraction. The coated Au sensor film was placed inside the system chamber and wavelength scan shows the nanoplasmonic peak position of a sensor is located at 800 nm-900 nm depending on the Au discs size and discs spacing. The Au nanodiscs, which act as optical antennas respond to events occurring at the interface between the sensor surface and sample material. A peak-fitting method proposed by Dahlin et al. [25] is applied to enable monitoring the spectral shifts on the order of 1 nm or less with a 0.01 nm resolution limit.

Preprints (www.preprints.org) | NOT PEER-REVIEWED | Posted: 7 September 2018 doi:10.20944/preprints201809.0124.v1

A fresh pure solvent was injected via the system pump to flush the tubes and to take a baseline measurement as settings are set at continuous, optimum flow rate of 0.1 µL/min to avoid bulk concentration gradient. At this point, minor spectral shifts were observed in both nanoplasmonic peak position and extinction due to change in the dielectric constant of the medium near the sensors. Upon diffusion of CH_3NH_3I into mesoporous TiO_2 film at the different concentrations and temperatures, the refractive index at Au nanodiscs changes with film color change (dark brown), known of perovskite reaction, as major spectral shifts of resonance wavelength and extinction of the previously located, sensor-specific peak, are simultaneously, in real time collected and monitored via Insplorer software. We have evaluated the injection time in the current study from the starting point of MAI injection until the nanoplasmonic peak has plateaued, corresponding to the transition stage in Figs. 1(a), 4(a). Typical time scale ranging from 18 s to 57 s has been calculated for the thinner 350 nm TiO_2 films, depending on MAI concentration used and operating temperature. Much prolonged injection time was observed in case of thicker 650 nm films with a range from 31 s up to 120 s [20]. In the standard sequential deposition method, 20 s dipping time has been applied using the 10 mg/mL MAI concentration under stagnant conditions [1]. The corresponding injection time in our study for the same MAI concentration (under continuous flow conditions) was 22 s.

For comparison, fresh solvent can be pumped again for rinsing the films. The sensors were removed for characterization. X-ray diffraction (XRD), Bruker AXS D4 Endeavour X diffractometer using Cu $K\alpha_{1/2}$, $\lambda\alpha_1$=154.060 pm, $\lambda\alpha_2$=154.439 pm radiation, was used to obtain XRD measurements on different substrates to probe perovskite phase formation as well as content of reactants and products. As indicated in, Fig. S1, the control samples show peaks of tetragonal

Preprints (www.preprints.org) | NOT PEER-REVIEWED | Posted: 7 September 2018 doi:10.20944/preprints201809.0124.v1

MAI at 2θ = 19.74° and 29.79° along with a hexagonal PbI_2 at 2θ = 12.8°. The XRD patterns on different substrate surfaces were acquired as control samples. As complementary characterizing technique, scanning electron microscopy (SEM) (JEOL-6300F, 5 kV), was used to obtain SEM images, which were analyzed using Image J software to generate histograms of particle size distributions.

3. Results and Discussion

3.1 Effect of MAI concentration on mesoporous TiO_2 *films*

The effect of changing MAI concentrations from 5 to 15 mg/mL at a high temperature of 41 °C on NPS response using Au sensors/compact TiO_2/350 nm mesoporous TiO_2/PbI_2 was evaluated. Fig.1 (a, b) and Fig.S1 (a) show the characteristic curves of nanoplasmonic peak position shifts and peak extinction shifts using 350 nm TiO_2 films. Fig.1 (a, b) show blue, fast shifts (higher rate constants) in the nanoplasmonic peak position for all concentrations except for the intermediate MAI concentration level at 10 mg/mL, which exhibits a red, slow shift (lower rate constant). The characteristic curves in Fig.S1 (a) depict the opposite behavior in nanoplasmonic peak extinction for all concentrations.

The perovskite formed at MAI concentrations of 5 mg/mL show smaller crystalline structures, Fig.2 (a), due to the fast conversion of 85 s^{-1}, Fig.1 (b). The MAI concentration of 5 mg/mL shows the highest intensity of XRD diffraction peaks at 2θ = 14.25°, 28.57°, Fig 3 (c-d). Hence, perovskite conversion was achieved using low MAI concentration by lowering the reaction activation energy (operating at temperature of 41 °C). The perovskite formed at other MAI concentrations of 7.5 mg/mL and 12.5 mg/mL show similar results, Fig S3. However, the MAI concentration of 7.5 mg/mL shows dense, small crystalline morphology with highest rate constant

Preprints (www.preprints.org) | NOT PEER-REVIEWED | Posted: 7 September 2018 doi:10.20944/preprints201809.0124.v1

of 125 s^{-1} where XRD diffraction peaks show highest residual unreacted PbI_2 at 2θ = 12.8°, Fig. 3 (b).

The perovskite formed at the 10 mg/mL MAI concentration and 41 °C is largely in cubic and nanowire form, Fig 2 (c), with slow and maximum conversion seen in NPS rate constant of 3.4 s^{-1}, Fig.1 (b), and highest intensity of XRD diffraction peak at 2θ = 31.95°, Fig 3 (e), respectively. The perovskite formed at MAI concentration of 15 mg/ml show similar morphology (nanowires and sheets with higher particle size distribution, Fig. S3 (e)) to the 10 mg/mL with a rate constant of 50 s^{-1} where XRD diffraction peaks show highest residual of MAI at 2θ = 19.74°, Fig 3 (a). It is noticeable that the slower reactions that allow growth in multi-dimensions such as those at MAI concentrations of 10 and 15 mg/mL are reflected by red or minimum blue NPS shifts.

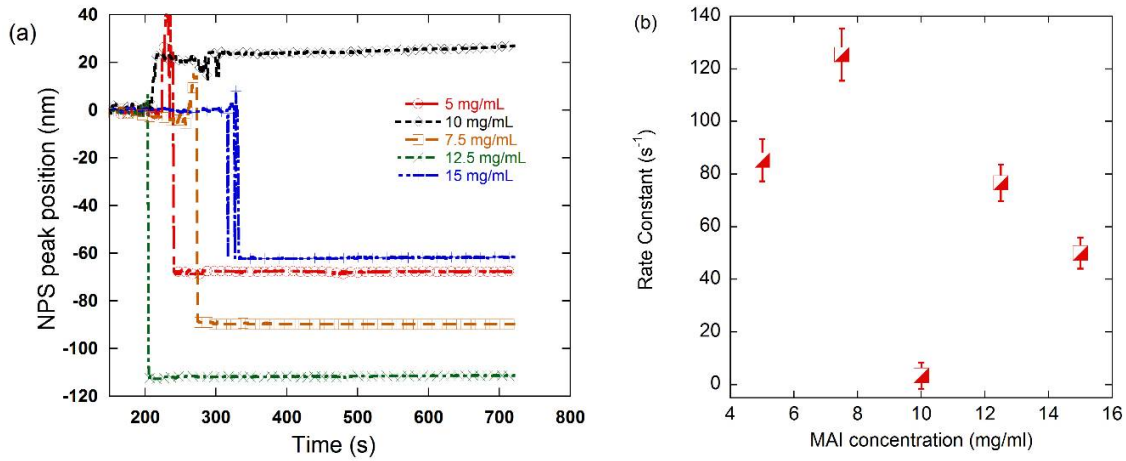

Figure 1. Characteristic MAI concentration curves measured for Au sensors/compact TiO_2/350 nm mesoporous TiO_2/PbI_2 prepared by continuous spin coating program showing (a) the nanoplasmonic peak position shifts for MAI concentrations ranging from 5 to 15 mg/mL at 41 °C and (b) the rate constants derived from the NPS peak position shifts. Both red and blue shifts are presented as positive rate constants.

Preprints (www.preprints.org) | NOT PEER-REVIEWED | Posted: 7 September 2018 doi:10.20944/preprints201809.0124.v1

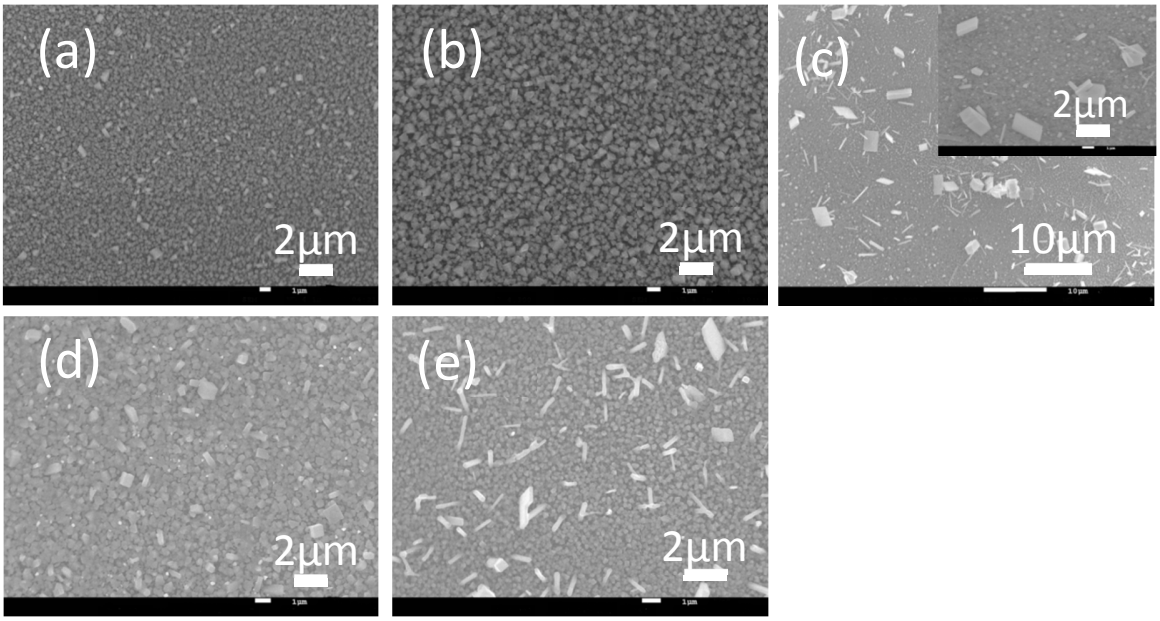

Figure 2. Typical SEM images of as-formed perovskites at different MAI concentrations; (a) 5, (b) 7.5, (c) 10, (d) 12.5 and (e) 15 mg/mL. Inset is shown for image (c) (at 10 mg/mL). The SEM images taken at different MAI concentrations for the 350 nm films revealed well-crystalline phase formation with different crystal morphologies.

Preprints (www.preprints.org) | NOT PEER-REVIEWED | Posted: 7 September 2018 doi:10.20944/preprints201809.0124.v1

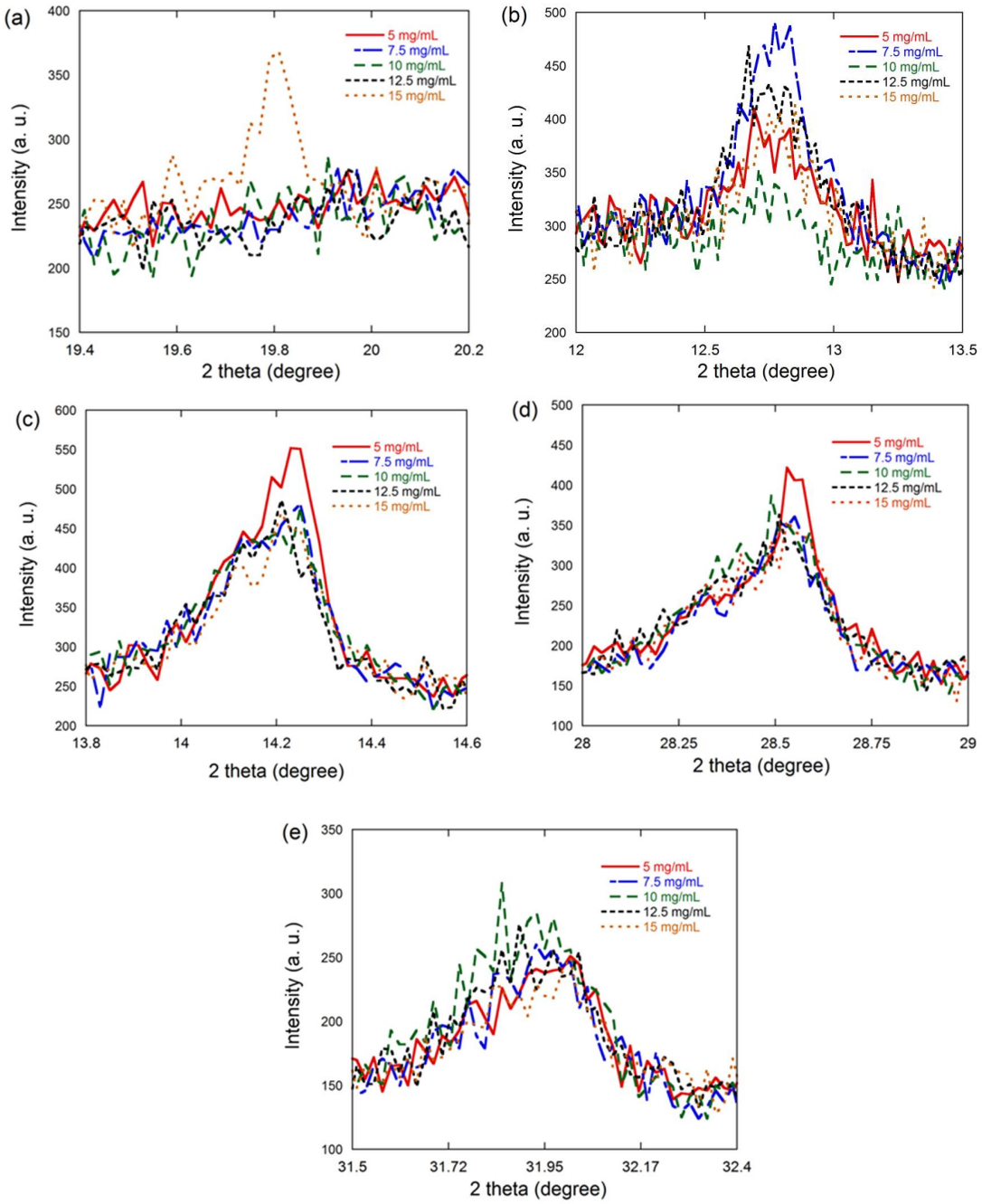

Figure 3. X-ray diffraction of Au sensors/compact TiO_2/thin mesoporous TiO_2/PbI_2 for varying MAI concentrations from 5-15 mg/mL at 41 °C. A series of diffraction peaks at 2θ = 14.25°, 28.57°, 31.95° corresponding to the tetragonal phase of $MAPbI_3$ perovskite have been detected at all MAI concentrations. MAI concentrations of 5.0 mg/mL shows highest peaks at 2θ = 14.25°, and at 2θ = 28.57°, while MAI concentration of 10 mg/mL shows highest peak at 2θ = 31.95°.

Preprints (www.preprints.org) | NOT PEER-REVIEWED | Posted: 7 September 2018 doi:10.20944/preprints201809.0124.v1

Tetragonal MAI at 2θ = 19.74° for MAI concentration of 15 mg/mL along with hexagonal PbI_2 at 2θ = 12.8° for MAI concentration of 7.5 mg/mL are maximum.

3.2 Effect of Temperature on mesoporous TiO_2 *films*

The effect of operating temperature (from 25 to 53 °C) at a fixed high MAI concentration of 12.5 mg/mL on NPS response for Au sensors/compact TiO_2/350 nm mesoporous TiO_2/PbI_2 was evaluated. Figure 4 (a, b) and Fig.S1 (b) show characteristic temperature curves on nanoplasmonic peak position shifts and peak extinction shifts using compact/350 nm mesoporous TiO_2 films. The characteristic curves in Fig. 4 (a, b) show red (positive) shifts of low rate constants of 3.4- 12 s^{-1} in the nanoplasmonic peak position for temperatures from 25-36 °C indicative of slow conversion. They also show blue (negative) shifts of higher rate constants of 34- 87 s^{-1} for temperatures from 41-53 °C indicative of fast conversion. The effect of changing the temperature on perovskite formation at high MAI concentration shows a non-linear relationship between the rate constant and temperature.

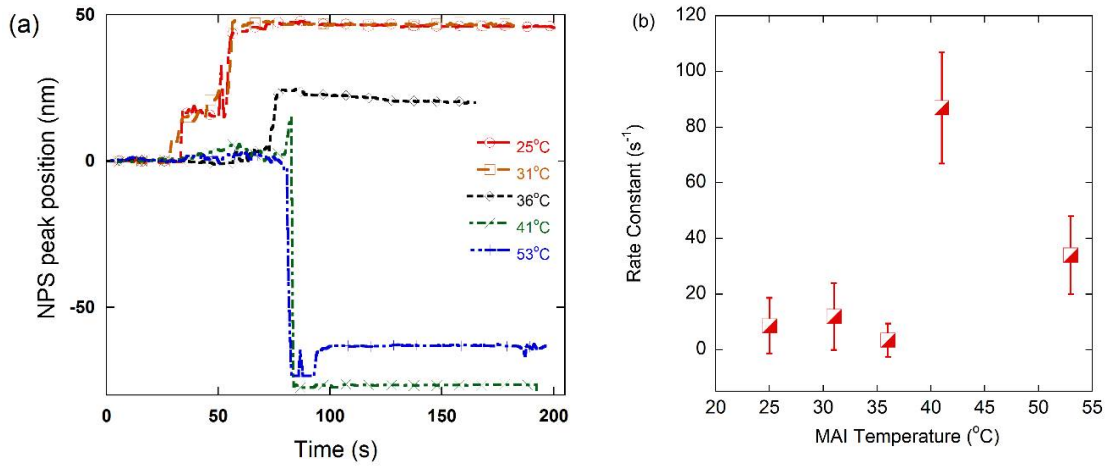

Preprints (www.preprints.org) | NOT PEER-REVIEWED | Posted: 7 September 2018 doi:10.20944/preprints201809.0124.v1

Figure 4. Characteristic temperature curves measured for Au sensors/compact TiO_2/350 nm mesoporous TiO_2/PbI_2 showing (a) the nanoplasmonic peak position shifts for temperatures ranging from 25 to 53 °C at MAI concentration of 12.5 mg/mL and (b) the rate constants derived from the NPS peak position shifts. Both red and blue shifts are presented as positive rate constants.

The conversion of PbI_2 with a dielectric constant ($\varepsilon\infty$=6) to $MAPbI_3$ perovskite with much higher ($\varepsilon\infty$~20)[26], Fig 5 (a-c), leads to the red shifts observed in NPS extinction at temperatures of 25-36 °C. However, the partial change in morphology from smooth (precursor PbI_2 film) to rough, sparse large crystals of MAI and $MAPbI_3$ perovskites, Fig 5 (d-e), reduces the contact area at the Au sensor interface leading to the blue shifts observed at temperatures of 41-53 °C.

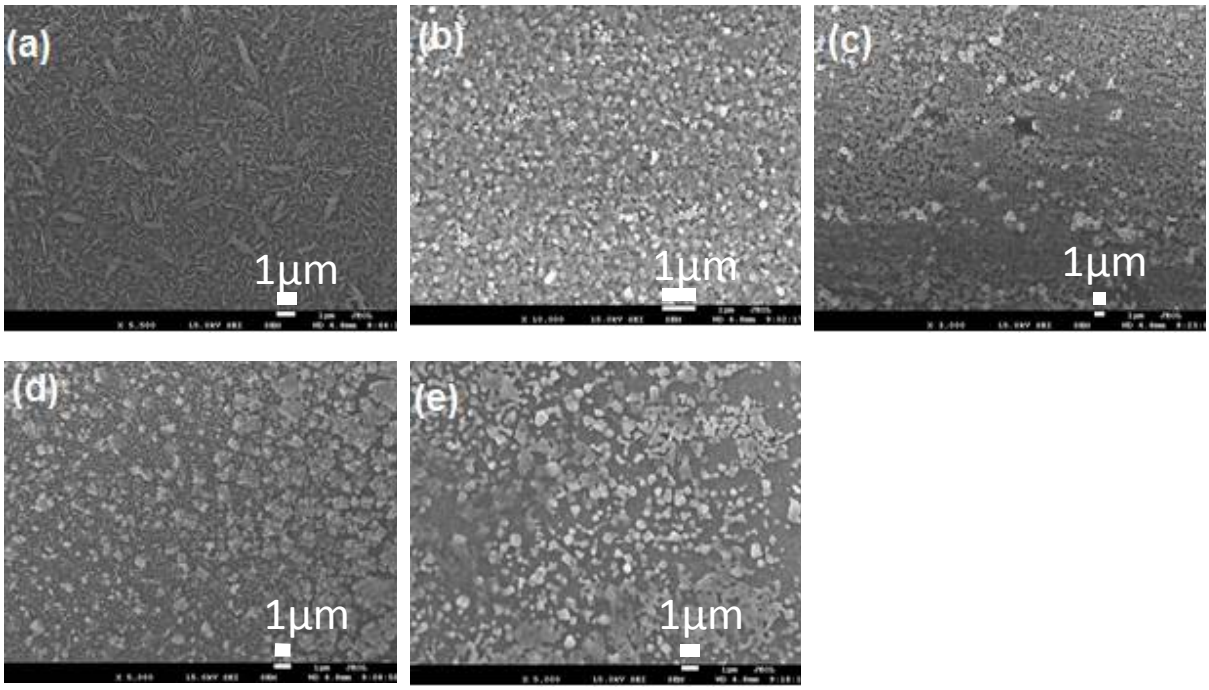

Figure 5. Typical SEM images of as-formed perovskites at different temperatures; 25, 31, 36, 41 and 53 ºC, respectively. The perovskite formed at (a) 25°C is leaf-like flakes of perovskite. The perovskite formed at (b-c) 31-36 °C show interconnected particles. The

 doi:10.20944/preprints201809.0124.v1

perovskite formed at (d-e) 41-53 °C show non-uniform formation of large and scattered crystals.

4. Conclusions

MAI injections at varying conditions to confined PbI_2 crystals can be monitored and recorded as red or blue shifts as seen by the formation of perovskites of various geometries. The change in dielectric constants of the materials upon injection of MAI into the Au sensor-coated TiO_2/PbI_2 films provides insight on the interface interactions and subsequently the ensemble peak pattern of the gold nanosensors can result in red or blue NPS shifts indicating perovskite conversion. While red shifts indicate slow reactions with multi-dimensional shapes, blue shifts showed faster reactions with lower conversions. By varying operation conditions, various perovskite structures can be synthesized and predicted utilizing their NPS responses.

Supporting Information

Additional NPS characterization, XRD, and SEM analysis

Acknowledgement

Authors would like to acknowledge the support of the Ministry of Higher Education, Kingdom of Saudi Arabia for this research under the Promising Centre for Sensors and Electronic Devices (PCSED) at Najran University, Kingdom of Saudi Arabia.

Conflict of Interest

The author declares there is not conflict of interest.

References

1. Burschka, J.; Pellet, N.; Moon, S.-J.; Humphry-Baker, R.; Gao, P.; Nazeeruddin, M. K.; Grätzel, M., Sequential Deposition as a Route to High-Performance Perovskite-Sensitized Solar Cells. *Nature* **2013**, *499*, 316-319.
2. Yang, W. S., et al., Iodide Management in Formamidinium-Lead-Halide–Based Perovskite Layers for Efficient Solar Cells. *Science* **2017**, *356*, 1376-1379.
3. Hu, Q.; Wu, J.; Jiang, C.; Liu, T.; Que, X.; Zhu, R.; Gong, Q., Engineering of Electron-Selective Contact for Perovskite Solar Cells with Efficiency Exceeding 15%. *ACS Nano* **2014**, *8*, 10161-10167.
4. deQuilettes, D. W.; Vorpahl, S. M.; Stranks, S. D.; Nagaoka, H.; Eperon, G. E.; Ziffer, M. E.; Snaith, H. J.; Ginger, D. S., Impact of Microstructure on Local Carrier Lifetime in Perovskite Solar Cells. *Science* **2015**, 348 (6235), 683-686.
5. Im, J.-H.; Jang, I.-H.; Pellet, N.; Grätzel, M.; Park, N.-G., Growth of $CH_3NH_3PbI_3$ Cuboids with Controlled Size for High-Efficiency Perovskite Solar Cells. *Nature Nanotechnology* **2014**, *9*, 927.
6. Saliba, M., et al., A Molecularly Engineered Hole-Transporting Material for Efficient Perovskite Solar Cells. *Nature Energy* **2016**, *1*, 15017.
7. Kojima, A.; Teshima, K.; Shirai, Y.; Miyasaka, T., Organometal Halide Perovskites as Visible-Light Sensitizers for Photovoltaic Cells. *J. Am. Chem. Soc.* **2009**, *131*, 6050-6051.
8. Zhang, T.; Yang, M.; Zhao, Y.; Zhu, K., Controllable Sequential Deposition of Planar $CH_3NH_3PbI_3$ Perovskite Films Via Adjustable Volume Expansion. *Nano Lett.* **2015**, *15*, 3959-3963.
9. Jeon, N. J.; Noh, J. H.; Kim, Y. C.; Yang, W. S.; Ryu, S.; Seok, S. I., Solvent Engineering for High-Performance Inorganic–Organic Hybrid Perovskite Solar Cells. *Nature Materials* **2014**, *13*, 897.
10. Patel, J. B.; Milot, R. L.; Wright, A. D.; Herz, L. M.; Johnston, M. B., Formation Dynamics of $CH_3NH_3PbI_3$ Perovskite Following Two-Step Layer Deposition. *J. Phys. Chem. Lett.* **2016**, *7*, 96-102.
11. Docampo, P.; Hanusch, F. C.; Stranks, S. D.; Döblinger, M.; Feckl, J. M.; Ehrensperger, M.; Minar, N. K.; Johnston, M. B.; Snaith, H. J.; Bein, T., Solution Deposition-

 doi:10.20944/preprints201809.0124.v1

Conversion for Planar Heterojunction Mixed Halide Perovskite Solar Cells. *Adv. Energy Mater.* **2014**, *4*, 1400355.

12. Liu, D.; Kelly, T. L., Perovskite Solar Cells with a Planar Heterojunction Structure Prepared Using Room-Temperature Solution Processing Techniques. *Nature Photonics* **2013**, *8*, 133.
13. Zhang, H.; Qiao, X.; Shen, Y.; Moehl, T.; Zakeeruddin, S. M.; Gratzel, M.; Wang, M., Photovoltaic Behavior of Lead Methylammonium Triiodide Perovskite Solar Cells Down to 80 K. *J. Mater. Chem. A* **2015**, *3*, 11762-11767.
14. Xiao, Z.; Zhao, L.; Tran, N. L.; Lin, Y. L.; Silver, S. H.; Kerner, R. A.; Yao, N.; Kahn, A.; Scholes, G. D.; Rand, B. P., Mixed-Halide Perovskites with Stabilized Bandgaps. *Nano Letters* **2017,** *17* (11), 6863-6869.
15. Saliba, M.; Tan, K. W.; Sai, H.; Moore, D. T.; Scott, T.; Zhang, W.; Estroff, L. A.; Wiesner, U.; Snaith, H. J., Influence of Thermal Processing Protocol Upon the Crystallization and Photovoltaic Performance of Organic–Inorganic Lead Trihalide Perovskites. *J. Phys. Chem. C* **2014**, *118*, 17171-17177.
16. Liu, M.; Johnston, M. B.; Snaith, H. J., Efficient Planar Heterojunction Perovskite Solar Cells by Vapour Deposition. *Nature* **2013**, *501*, 395.
17. Nie, W., et al., High-Efficiency Solution-Processed Perovskite Solar Cells with Millimeter-Scale Grains. *Science* **2015**, *347*, 522.
18. Shi, D., et al., Low Trap-State Density and Long Carrier Diffusion in Organolead Trihalide Perovskite Single Crystals. *Science* **2015**, *347*, 519.
19. Li, D.; Cui, J.; Li, H.; Huang, D.; Wang, M.; Shen, Y., Graphene Oxide Modified Hole Transport Layer for $CH_3NH_3PbI_3$ Planar Heterojunction Solar Cells. *Solar Energy* **2016**, *131*, 176-182.
20. Rajab, F.; Harraz, F., Real Time Nanoplasmonic Sensing for Monitoring $CH_3NH_3PbI_3$ Perovskite Formation in Mesoporous TiO_2 Films. *Journal of Crystal Growth*. (under review)
21. Gusak, V.; Heiniger, L.-P.; Graetzel, M.; Langhammer, C.; Kasemo, B., Time-Resolved Indirect Nanoplasmonic Sensing Spectroscopy of Dye Molecule Interactions with Dense and Mesoporous TiO_2 Films. *Nano Lett.* **2012**, *12*, 2397-2403.

 doi:10.20944/preprints201809.0124.v1

22. Gusak, V.; Heiniger, L.-P.; Zhdanov, V. P.; Gratzel, M.; Kasemo, B.; Langhammer, C., Diffusion and Adsorption of Dye Molecules in Mesoporous TiO_2 Photoelectrodes Studied by Indirect Nanoplasmonic Sensing. *Energy Environ. Sci.* **2013**, *6*, 3627-3636.
23. Larsson, E. M.; Langhammer, C.; Zorić, I.; Kasemo, B., Nanoplasmonic Probes of Catalytic Reactions. *Science* **2009**, *326*, 1091.
24. Langhammer, C.; Larsson, E. M.; Kasemo, B.; Zorić, I., Indirect Nanoplasmonic Sensing: Ultrasensitive Experimental Platform for Nanomaterials Science and Optical Nanocalorimetry. *Nano Lett.* **2010**, *10*, 3529-3538.
25. Dahlin, A. B.; Tegenfeldt, J. O.; Höök, F., Improving the Instrumental Resolution of Sensors Based on Localized Surface Plasmon Resonance. *Anal. Chem.* **2006**, *78*, 4416-4423.
26. Du, M. H., Efficient Carrier Transport in Halide Perovskites: Theoretical Perspectives. *J. Mater. Chem. A* **2014**, *2*, 9091-9098.